Raman Studies of Structural Changes in Diamond-like Carbon Films on Si Induced by Ultrafast Laser Ablation

Keisuke Takabayashi[1], Khaidir Bin Khamaron[1], Takuro Tomita[2], Takashi Takahashi[3], Yohei Kobayashi[3], Makoto Yamaguchi[*1]

[1]Graduate School of Engineering Science, Akita University, Japan
[2]Graduate School of Sciences and Technology for Innovation, Tokushima University, Japan
[3]The Institute for Solid State Physics, University of Tokyo, Japan
[*]Corresponding author's e-mail: yamaguci@phys.akita-u.ac.jp

In this study, the diamond-like carbon (DLC), a tetrahedral amorphous carbon sample deposited on Si, was irradiated using a picosecond laser. We evaluated the picosecond-laser-induced structural and morphological changes in DLC using micro-Raman spectroscopy via line measurements. We obtained the spatial distribution of the structure and morphology of DLC on Si by regression analysis of the Raman spectra. The photo-induced crater could be categorized into four regions: peripheral, morphological-change, structural-changes, and ablated regions. The structure and morphology of the peripheral region were similar to those of the as-received DLC. In the morphological-change region, which is inside the periphery region, the thickness of the DLC decreased without any structural changes. At the center of the crater, which is shown in black in the optical image, two regions were identified by Raman spectroscopy. On the outer side, there is a structural-change region where the graphitization of DLC materialized with a reduction in the film thickness. Inside the structural-change region, there is an ablated region where the DLC was degraded by laser ablation.

1. Introduction

Recently, laser processing garnered significant interest owing to its processing capability of high-quality materials. The dominant factor in the laser processing mechanism depends on the pulse duration and fluence of the irradiating laser. In laser processing with nanosecond pulses, thermal processes are dominant, and the materials are processed through melting or evaporation. In femtosecond-laser processing, the non-thermal process becomes dominant because the laser pulse duration is comparable to the electron-lattice interaction time. Because a significant energy is injected in a very short time, unique phenomena such as structural change [1], high-precision processing, and laser-induced periodic structures [2–5], can be observed. However, it is challenging to distinguish between thermal and non-thermal processes, and the cumulative interaction of these two effects results in various phenomena. The regulation of these effects can lead to precise and advanced laser processing applications.

Numerous studies on the structural changes in carbon induced by laser irradiation have been reported [6–11]. Quenched carbon (Q-carbon), which undergoes structural changes from a diamond-like carbon (DLC) film and new phase of amorphous carbon, was discovered in 2015 [6]. It has interesting properties, such as room-temperature ferromagnetism and grater hardness than that of diamond. The formation of silicon carbide (SiC) nanocrystals by femtosecond laser pulses on amorphous carbon films deposited on Si has been reported [7]. Furthermore, new phases with novel properties and laser-induced structural changes via a simpler method are anticipated to be discerned.

Laser-induced phenomena are affected by laser parameters, such as wavelength, pulse duration, fluence, and repetition rate; however, the effects remain not entirely understood. Many studies have been performed to elucidate the effects of the laser parameters. Takahashi et al. developed an automatic pulse-duration-tunable laser system and observed two ablation thresholds of Si at a fluence of 0.22 J/cm^2 with a pulse duration below 4 ps and at an intensity of 24 GW/cm^2 above 13 ps [12]. Yoshinaka et al. investigated the relationship between the energy density of pulsed laser annealing and sp^3 content in the formed Q-carbon [8]. Discerning the laser-induced mechanism is essential to determine its dependence on laser parameters.

In this study, photo-induced structural changes of DLC films on Si were evaluated via micro-Raman spectroscopy, which cannot be determined using only optical imagery. A picosecond laser with a pulse duration of 5 ps and fluence of 10 J/cm^2 was applied to the DLC surface. Raman spectroscopy is a non-destructive and non-contact method for characterizing the structure of a sample, where the scattered light is used to measure the vibrational levels. Furthermore, it is advantageous in evaluating the physical properties of carbon materials with various allotropes. Line measurements across the center of the laser-irradiated crater were performed to evaluate the spatial distribution of the structural changes. Numerous materials are composed of carbon atoms, such as diamond, graphite, and graphene, which have different bonding properties. Subsequently, we consider the production of a new carbon material using DLC, which consists of sp^2 and sp^3 bonds. To control the structural changes in the

carbon films induced by the laser, we evaluated the photo-induced structural changes in DLC.

2. Materials and Methods
2.1 Materials

A DLC film with a high sp^3 content and hydrogen-free tetrahedral amorphous carbon (ta-C) [13] was used as the test sample. The film was deposited on a silicon substrate with a thickness of approximately 100 nm and irradiated using ytterbium-doped fiber laser with a wavelength of 1.03 μm, repetition rate of 1 MHz, accumulated pulse number of 10^5 shots, pulse duration of 5 ps, and fluence of 10 J/cm^2. The laser beam was focused on a spot size of approximately 5 μm on the DLC film surface. Laser irradiation was performed at room temperature in an atmospheric environment.

2.2 Raman spectroscopy

Micro-Raman spectroscopy (Horiba, LabRam HR Evolution) was performed in the range of 200–1800 cm^{-1} with a spectral resolution of 4 cm^{-1} at room temperature. The excitation wavelength was set to 355 nm. A 40× objective lens was used to focus, and the diameter of the laser spot was approximately 1 μm. Therefore, the spatial resolution was estimated to be 1 μm. Line measurements were performed across the center of the crater. The distance between the measured points was 0.5 μm.
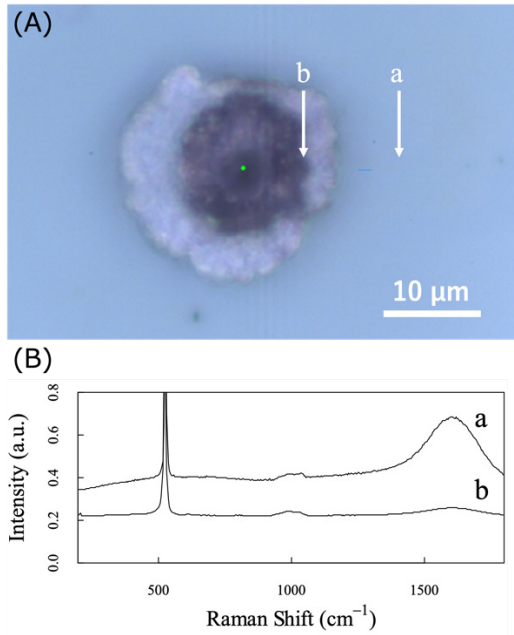
3. Results and discussion

Fig. 1 (A) The optical image of the irradiated crater with the peak fluence of 10 J/cm^2 and pulse duration of 5 ps and (B) Raman spectra at points a and b. Raman spectra were normalized with the intensity of Si (520 cm^{-1}). The peak due to DLC (1600 cm^{-1}) at point b is weaker than that at point a.

Figure 1 (A) presents an optical image of a laser-irradiated crater. The Raman spectra are shown in Figure 1 (B). The spectra depicted a normalized intensity of approximately 520 cm^{-1}. Spectra a and b presented in Fig. 1 (B) are the spectra at points a and b, as indicated in Fig. 1 (A). The

peaks occurring at approximately 520 and 1000 cm^{-1} are attributed to the first-and second-order phonons of the silicon substrate, respectively [14]. The peak occurring at approximately 1600 cm^{-1} was because to the DLC film. The spectra at point a are similar to those of the as-received (unirradiated region) sample. This indicates that structural changes due to laser irradiation did not occur at point a. However, at point b, structural changes occurred owing to the irradiation process.

Regression analysis was performed to analyze the spectral intensity and shape in a range of 900–1800 cm^{-1}. The Levenberg-Marquardt algorithm was used for the analysis (R language, minpack library). The full width at half maximum of each Raman peak was considered constant. Several typical spectra were fitted preliminarily and their results were utilized. The Lorentzian, Gaussian, asymmetric pseudo-Voigt function, and linear functions were used for spectral fitting. The functions used in this study are specified in Equations (1)–(4), where, ω, I, ω_0, and Δ are the Raman shift, peak intensity, central value of the wavenumber, and full width at half maximum of the peaks, respectively. The parameter m is the combination ratio of the Gaussian and Lorentzian functions, which can be between 0 and 1.

$$f_{\text{Lorenz}}(\omega; I, \omega_0, \Delta) = \frac{I \times (\Delta/2)^2}{(\omega - \omega_0)^2 + (\Delta/2)^2} \quad (1)$$

$$\begin{aligned}&f_{\text{Gauss}}(\omega; I, \omega_0, \Delta)\\ &= I \times \exp\left[-4\log 2 \times \left(\frac{\omega - \omega_0}{\Delta}\right)^2\right]\end{aligned} \quad (2)$$

$$\begin{aligned}&f_{\text{pVoigt}}(\omega; I, \omega_0, \Delta, m)\\ &= m f_{\text{Lorenz}} + (1-m) f_{\text{Gauss}}\end{aligned} \quad (3)$$

$$\begin{aligned}&f_{\text{asym-pVoigt}}(\omega; I, \omega_0, \Delta_1, \Delta_2, m_1, m_2)\\ &= \begin{cases} f_{\text{pVoigt}}(\omega; I, \omega_0, \Delta_1, m_1), & \omega < \omega_0 \\ f_{\text{pVoigt}}(\omega; I, \omega_0, \Delta_2, m_2), & \omega \geq \omega_0 \end{cases}\end{aligned} \quad (4)$$
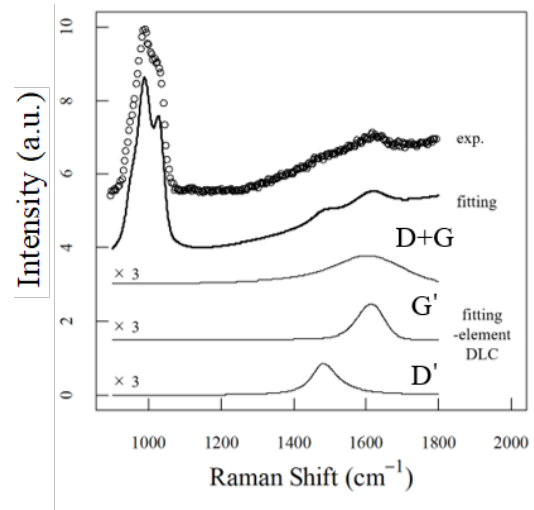

Fig. 2 Fitted curve in the range of 900–1800 cm^{-1}. The snv spectrum (exp.), fitting example, and fitting elements due to DLC (D+G, G' and D') are shown. Fitting elements are shown in triplets.

The fitting model function consists of 10 sub-functions. The Raman signal from the DLC film can be modeled as asymmetric pseudo-Voigt functions, denoted as D + G, D',

and G'. The Raman spectrum of a typical DLC film has G and D peaks owing to sp^2 and defects [13]. These two peaks were combined and modeled with an asymmetric pseudo-Voigt function, denoted as the D + G peak. The D and G peaks following the structural change are denoted as the D' and G' peaks, respectively. This structural change is due to the graphitization of the DLC film, which is evident because the D' and G' peaks could be observed independently after irradiation. However, the two peaks overlapped and could not be distinguished in the as-received film. The peak due to the second-order of Si (1000 cm^{-1}) was modeled by a combination of four Gaussian and Lorentzian functions. The intensity of the baseline increases near the center of the crater. The baselines at the low and high wavenumber sides can be attributed to the amorphization of the silicon substrate and photoluminescence, respectively. The baseline is modeled by a combination of a linear function and two Lorentzian functions.

The product of I and Δ obtained following the fitting is considered as the peak area, as detailed in Equations (5)–(9). The areas of the D + G, D', and G' peaks, which are asymmetric pseudo-Voigt functions, are denoted as A_{D+G}, $A_{D'}$, and $A_{G'}$, respectively, as stated in Equations (5)–(7). The sum of the areas of all peaks is denoted as A_{DLC}, as given in Equation (8). The area of the second-order Si is denoted as A_{Si}, as shown in Equation (9).

$$A_{D+G} = I_{D+G} \times \left(\frac{\Delta_{D+G,1}}{2} + \frac{\Delta_{D+G,2}}{2} \right) \qquad (5)$$

$$A_{D'} = I_{D'} \times \left(\frac{\Delta_{D',1}}{2} + \frac{\Delta_{D',2}}{2} \right) \qquad (6)$$

$$A_{G'} = I_{G'} \times \left(\frac{\Delta_{G',1}}{2} + \frac{\Delta_{G',2}}{2} \right) \qquad (7)$$

$$A_{DLC} = A_{D+G} + A_{D'} + A_{G'} \qquad (8)$$

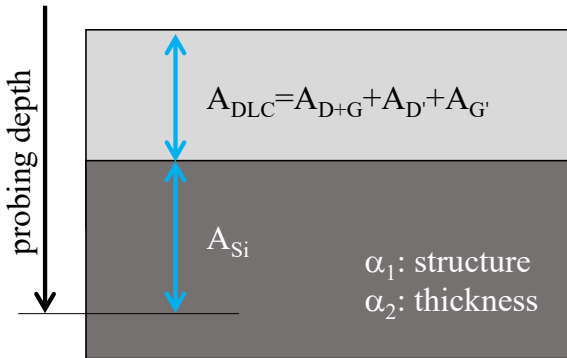$$A_{Si} = \sum_i^4 A_{Si,i} = \sum_i^4 I_{Si.i} \times \Delta_{Si.i} \qquad (9)$$

Fig. 3 The relationship between the total peak area and thickness or structure of DLC film.

The ratios of A_{D+G} to A_{DLC} and A_{DLC} to A_{Si} are denoted as α_1 and α_2, respectively, as stated in Equations (10) and (11), respectively. A_{DLC}/A_{Si} is normalized by one of the as-received films, as shown in Equation (11). α_1 and α_2 corre-

spond to the structure and thickness of the DLC film, respectively. Figure 3 depicts the relationship between the Raman spectrum and thickness or structure of the DLC film. The total peak area obtained by integrating the area of all peaks in the spectrum was proportional to the amount of material present in the measured region.

$$\alpha_1 = \frac{A_{D+G}}{A_{DLC}} \qquad (10)$$

$$\alpha_2 = \frac{A_{DLC}/A_{Si}}{(A_{DLC}/A_{Si})_{as\ received}} \qquad (11)$$

The position dependences of α_1 and α_2 are shown in Fig. 4. The dashed and solid lines represent α_1 and α_2, respectively. The position dependences of α_1 and α_2 exhibit variations. As indicated by the arrows in Fig. 4, the change in α_2 starts farther from the center of the crater compared to the change in α_1. This indicates that the variation in thickness started from the outside of the crater (region 2). A structural change occurred near the center of the crater (region 3). At the crater center (region 4), no peak was observed because the DLC film was completely removed by laser ablation.
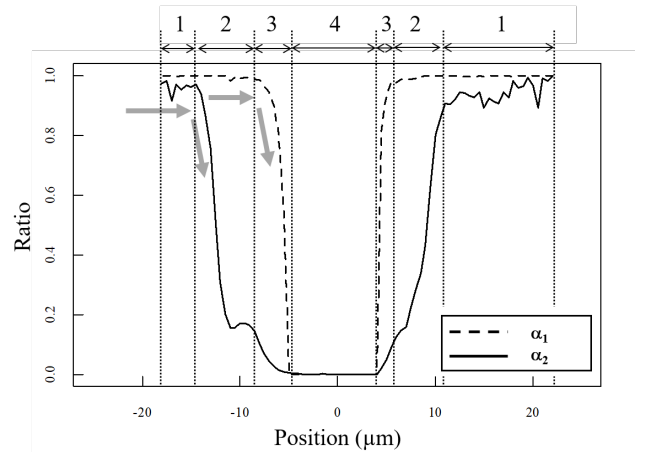

Fig. 4 Position dependence on the area ratio. We classify regions 1–4 based on thickness and structure change.

Table 1 Labeled regions based on fitting result and their details. As rec. expresses that the structure and thickness are the same those of the as-received films.

region	1. (Periphery)	2. (Morpho-logical change)	3. (Structural change)	4. (Ablated)
α_1	Const.	Const.	decreased	-
α_2	Const.	decreased	decreased	0
Structure	As rec.	As rec.	graphitized	-
Thickness	As rec.	decreased	decreased	removed

A summary of the Raman analysis results and regions labeled based on the regression analysis are reported in Table 1. In the periphery region (1), which is the farthest region from the laser-focused crater, the structure and thickness of the DLC film were similar to those of the as-received film. In this region, there was no change due to the laser irradia-

tion. In the region of morphological change (2), which is inside the periphery region, the thickness of the DLC film decreased; however, no structural changes were observed. In the region of structural change (3), which is inside the morphological-change region, the thickness of the DLC film decreased, and graphitization of the film occurred. In the ablated region (4), which is inside the structural change region, the DLC peak was not observed. We conclude that the DLC film was effectively removed by laser irradiation.

Next, the correlation between the optical images and Raman spectra is discussed. Three different regions are observed in the optical image: the black region at the center of the image, white region enveloping the black region, and blue region encompassing the white region. The structural change and ablated regions determined from the Raman spectra correspond to the black region. The morphological-change region corresponds to white and the periphery corresponds to blue in the optical image. The structural changes and ablated regions cannot be visualized on the optical image.

The predominant effect of laser irradiation on Si is amorphization [15]. The Raman characterization of a-Si was reported by Wu et al. [16]. In our study, only a small trace of amorphous Si was observed. The amorphization of crystal Si decreased the intensity of the Si peak. Therefore, α_2 increases. Because we did not observe a significant increase in α_2, we were certain of the degradation of DLC.
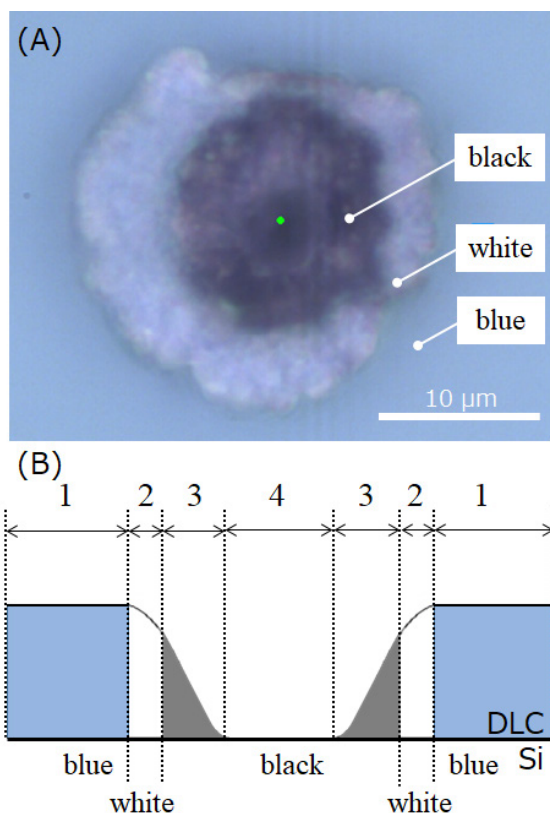

Fig. 5 (A) Irradiation crater with 5 ps, 10 J/cm² and (B) DLC image after structural and morphological changes.

Surface swelling, multilevel spallation, and graphitization of DLC by laser irradiation have been reported in the literature [17–21]. In our study, swelling and spallation were not observed in the Raman spectra, thus, their effects on the profile were not considered. To further investigate the synthesized film, including the differences in the absorption coefficient, the incubation effects [22] caused by the difference in the number of pulses and effects of Si substrate are required.

4. Conclusions

A picosecond laser (λ = 1.03 μm, τ = 5 ps, E = 10 J/cm², 10^5 pulses) was irradiated on the surface of the DLC deposited on Si. We performed micro-Raman spectroscopy on this sample to investigate the local DLC film structure after laser irradiation. Line measurements via Raman spectroscopy were performed by exciting the sample at 355 nm. We performed spectral fitting of the Raman spectra and investigated the photo-induced structural and morphological changes. We obtained the spatial distribution of the structure and morphology of DLC on Si by regression analysis of the Raman spectra. The DLC film degraded, and the observed structural changes corresponded to a change in the optical image of the crater. The photo-induced film vicinity was categorized into four regions. The blue region in the optical image has a structure and morphology similar to that of the as-received DLC, and the white region is considered to be the morphological-change region without any structural change. The black region is considered to be the structural-change region with morphological changes; the DLC is graphitized in this region. In the center of the black region in the optical image, there are regions where the DLC deteriorated, which could not be observed in the optical image. This study is ongoing, and many effects, such as amorphization of substrate Si, surface swelling, spallation, and absorption coefficient are not considered. Therefore, further analyses are required.

References
[1] T. Okada, T. Tomita, H. Katayama, Y. Fuchikami, T. Ueki, H. Hisazawa, and Y. Tanaka: App. Phys. A, (2019) 125.
[2] T. Tomita, K. Kinoshita, S. Matsuo, and S. Hashimoto: Appl. Phys. Lett., 90, (2007) 153115.
[3] G. Miyaji and Miyazaki: Appl. Phys. Lett., 91, (2007) 123102.
[4] N. Yasumaru, K. Miyazaki, and J. Kiuchi: Appl. Surf. Sci., 254, (2008) 2364.
[5] M. Yamaguchi, S. Ueno, R. Kumai, K. Kinoshita, T. Murai, T. Tomita, S. Matsuo, and S. Hashimoto: Appl. Phys. A, 99, (2010) 23.
[6] J. Narayan and A. Bhaumik: J. Appl. Phys., 118, (2015) 215303.
[7] S. Toth, P, Nemeth, P. Racz, L. Himics, P. Dobi, and M. Koos: Diam. Relat. Mater., 81, (2018) 96.
[8] H. Yoshinaka, S. Inubushi, T. Wakita, T. Yokoya, and Y. Muraoka: Carbon, 167, (2020) 504.
[9] G. Dumitru, V. Romano, H.P. Weber, S. Pimenov, T. Kononenko, J. Hermann, S. Bruneau, Y. Gerbig, and M. Shupegiin: Diam. Relat. Mater., 12, (2003) 1034.

[10] V.V. Kononenko, A.A. Khomich, A.V. Khomich, R.A. Lhmelnitskii, V.M. Gololobov, M.S. Komlenok, A.S. Orekhov, A.S. Orekhov, and V.I. Konov: Appl. Phys. Lett., 114, (2019) 251903.

[11] J. Kanasaki, E. Inami, K. Tanimura, H. Ohnishi, and K. Nasu: Phys. Rev. Lett., 102, (2009) 087402.

[12] T. Takahashi, S. Tani, R. Kuroda, and Y. Kobayashi: Appl. Phys. A, 126, (2020) 582.

[13] A.C. Ferrari and J. Robertson: Phil. Trans. R. Soc. Lond. A, 362, (2004) 2477.

[14] P. Mishra and K.P. Jain: Phys. Rev. B, 64, (2001) 073304.

[15] F. Costache, S.K. Arguirova, and J. Reif: Appl. Phys. A, 79, (2004) 1429.

[16] K. Wu, X.Q. Yan, and M.W. Chen: Appl. Phys. Lett., 91, (2003) 101903.

[17] L. Marcinauskas, A. Grigonis, M. Geduilas, L. Vgricaite, G. Racvkaitis, Z. Rutkunene, and M. Cernauskas: J. Laser Micro Nanoeng., 10, (2015) 43.

[18] A. Grigonis, A. Medvid, P. Onufrijevs, J. Babonas, and A. Reza: Opt. Mater., 30, (2008) 749.

[19] T.V. Kononenko, S.M. Pimenov, V.V. Kononenko, E.V. Zavedev, V.I. Konov, G. Dumitru, and V. Romano: Appl. Phys. A, 79, (2004) 543.

[20] T.V. Kononenko. V.V. Kononenko, S.M. Pimenov, E.U. Zavedoev, U.I. Konov, V. Romano, and G. Dumitru: Diam. Relat. Mater., 14, (2005) 1368.

[21] G. Dumitru, V. Romano, H.P. Weber, S.M. Pimenov, T. Kononenko, M. Sentis, J. Hermann, and S. Bruneau: Appl. Surf. Sci., 222, (2004) 226.

[22] S. Tani and Y. Kobayashi: Appl. Phys. A, (2018) 124.